

The Probability Distribution of Binary Pulsar Coalescence Rates.

I. Double Neutron Star Systems in the Galactic Field

C. Kim¹, V. Kalogera¹ and D. R. Lorimer²

¹ Northwestern University, Dept. of Physics & Astronomy, 2145 Sheridan Rd., Evanston, IL 60208

² University of Manchester, Jodrell Bank Observatory, Macclesfield, Cheshire, SK11 9DL, UK.

c-kim1@northwestern.edu; vicky@northwestern.edu; drl@jb.man.ac.uk

ABSTRACT

Estimates of the Galactic coalescence rate (\mathcal{R}) of close binaries with two neutron stars (NS–NS) are known to be uncertain by large factors (about two orders of magnitude) mainly due to the small number of systems detected as binary radio pulsars. We present an analysis method that allows us to estimate the Galactic NS–NS coalescence using the current observed sample and, importantly, to assign a statistical significance to these estimates and to calculate the allowed ranges of values at various confidence levels. The method involves the simulation of selection effects inherent in all relevant radio pulsar surveys and a Bayesian statistical analysis for the probability distribution of \mathcal{R} . The most likely values for the total Galactic coalescence rate ($\mathcal{R}_{\text{peak}}$) lie in the range $2 - 60 \text{ Myr}^{-1}$ depending on different pulsar population models. For our reference model 1, where the most likely estimates of pulsar population properties are adopted, we obtain $\mathcal{R}_{\text{tot}} = 8_{-5}^{+9} \text{ Myr}^{-1}$ at a 68% statistical confidence level. The corresponding range of expected detection rates of NS–NS inspiral are $3_{-2}^{+4} \times 10^{-3} \text{ yr}^{-1}$ for the initial LIGO and $18_{-11}^{+21} \text{ yr}^{-1}$ for the advanced LIGO.

Subject headings: binaries: close—gravitational waves—stars: neutron

1. INTRODUCTION

The detection of the double neutron star (NS–NS) prototype PSR B1913+16 as a binary pulsar (Hulse & Taylor 1975) and its orbital decay due to emission of gravitational waves (Taylor et al. 1979) has inspired a number of quantitative estimates of the coalescence rate of NS–NS binaries (Clark et al. 1979; Narayan et al. 1991; Phinney 1991; Curran & Lorimer 1995).

In general, the coalescence rate of NS–NS binaries can be calculated based on: (a) our theoretical understanding of their formation (see Belczynski & Kalogera 2001 for a review and application of this approach); (b) the observational properties of the pulsars in the binary systems and the modeling of pulsar survey selection effects (see e.g. Narayan 1987). Interest in these coalescence derives from an intrinsic motivation of understanding their origin and evolution and their connections to other NS binaries. However, significant interest derives from their importance as gravitational-wave sources for the upcoming ground-based laser interferometers (such as LIGO) and their possible association with γ -ray burst events (Popham et al. 1998 and references therein).

The traditional way of calculating the coalescence rate based on observations involves an estimate of the *scale factor*, an indicator for the number of pulsars in our Galaxy with the same spin period and luminosity (Narayan 1987). Corrections must then be applied to these scale factors to account for the faint end of the pulsar luminosity function, the beamed nature of pulsar emission, and uncertainties in the assumed spatial distribution. The estimated total number in the Galaxy can then be combined with estimates of their lifetimes to obtain a coalescence rate, \mathcal{R} . This method was first applied by Narayan et al. (1991) and Phinney (1991) and other investigators who followed (Curran & Lorimer 1995; van den Heuvel & Lorimer 1996). Various correction factors were (or were not) included at various levels of completeness. Summaries of these earlier studies can be found in Arzoumanian et al. (1999) and Kalogera et al. (2001; hereafter KNST). The latter authors examined all possible uncertainties in the estimates of the coalescence rate of NS–NS binaries in detail, and pointed a small-number bias that introduces a large uncertainty (more than two orders of magnitude) in the correction factor for the faint-pulsar population that must be applied to the rate estimate. They obtained a total NS–NS rate estimate in the range $\mathcal{R} = 10^{-6} - 5 \times 10^{-4} \text{ yr}^{-1}$, with the uncertainty dominated by the small-number bias. Earlier studies, which made different assumptions about the pulsar properties (e.g. luminosity and spatial distributions and lifetimes), are roughly consistent with each other (given the large uncertainties). Estimated ranges of values until now were not associated with statistical significance statements and an “all-inclusive” estimated Galactic coalescence rate lies in the range $\sim 10^{-7} - 10^{-5} \text{ yr}^{-1}$.

The motivation for this paper is to update the scale factor calculations using the most recent pulsar surveys, and present a statistical analysis that allows the calculation of statistical confidence levels associated with rate estimates. We consider the two binaries found in the Galactic disk: PSR B1913+16 (Hulse & Taylor 1975) and PSR B1534+12 (Wolszczan 1991). Following the arguments made by Phinney (1991) and KNST, we do not include the globular cluster system PSR B2127+11C (Prince et al. 1991); this system will be the subject of a later paper. Radio-pulsar-survey selection effects are taken into account in the modeling of

pulsar population. As described in what follows, the small-number bias and the effect of a luminosity function are *implicitly included* in our analysis, and therefore a separate correction factor is not needed. For each population model of pulsars, we derive the probability distribution function of the total Galactic coalescence rate weighted by the two observed binary systems. In our results we note a number of important correlations between $\mathcal{R}_{\text{peak}}$ and model parameters that are useful in generalizing the method. We extrapolate the Galactic rate to cover the detection volume of LIGO and estimate the detection rates of NS–NS inspiral events for the initial and advanced LIGO.

The plan for the rest of this paper is as follows. In §2, we describe our analysis method in a qualitative way. Full details of the various pulsar population models and survey selection effects are then given in §3 and §4 respectively. In §5, we derive the probability distribution function for the total Galactic coalescence rate and calculate the detection rate of LIGO. In §6, we summarize our results and discuss a number of intriguing correlations between various physical quantities. Finally, in §7, we discuss the results and compare them with previous studies.

2. BASIC ANALYSIS METHOD

Our basic method is one of “forward” analysis. By this we mean that we do not attempt to invert the observations to obtain the total number of NS–NS binaries in the Galaxy. Instead, using Monte Carlo methods, we populate a model galaxy with NS–NS binaries (that match the spin properties of PSR B1913+16 and PSR B1534+12) with pre-set properties in terms of their spatial distribution and radio pulsar luminosity function. Details about these “physical models” are given in §3.

For a given physical model, we produce synthetic populations of different total numbers of objects (N_{tot}). We then produce a very large number of Monte Carlo realizations of such pulsar populations and determine the number of objects (N_{obs}) that are observable by all large-scale pulsar surveys carried out to date by detailed modeling of the detection thresholds of these surveys. This analysis utilizes code to take account of observational selection effects in a self-consistent manner, developed and described in detail by Lorimer et al. (1993; hereafter LBDH) which we summarize in §4. Performing this analysis for many different Monte Carlo realizations of the physical model allows us to examine the distribution of N_{obs} . We find, as expected and assumed by other studies, that this distribution closely follows Poisson statistics, and we determine the best-fit value of the mean of the Poisson distribution λ for each population model and value of N_{tot} .

The calculations described so far are performed separately for each of PSR B1913+16 and PSR B1534+12 so that we obtain separate best-fit λ values for the Poisson distributions. Doing the analysis in this way allows us to calculate the *likelihood of observing just one example of each pulsar in the real-world sample*. Given the Poissonian nature of the distributions this likelihood is simply: $P(1; \lambda) = \lambda \exp(-\lambda)$. We then calculate this likelihood for a variety of assumed N_{tot} values for each physical model.

The probability distribution of the total coalescence rate \mathcal{R}_{tot} is derived using the Bayesian analysis and the calculated likelihood for each pulsar (described in detail in §5). The derivation of this probability distribution allows us to calculate the most probable rate as well as determine its ranges of values at various statistical confidence levels. Finally, we extrapolate the Galactic rate to the volume expected to be reached by LIGO and calculate the detection rate, \mathcal{R}_{det} (see §6).

3. MODELS FOR THE GALACTIC PULSAR POPULATION

Our model pulsar populations are characterized by a Galactocentric radius (R), vertical distance (Z) from the Galactic plane and radio luminosity (L). Assuming that the distributions of each of these parameters are independent, the combined probability density function (PDF) of the model pulsar population can be written as:

$$f(R, Z, L) dR dZ dL = \psi_R(R) 2\pi R dR \psi_Z(Z) dZ \phi(L) dL, \quad (1)$$

where $\psi_R(R)$, $\psi_Z(Z)$ and $\phi(L)$, are the individual PDFs of R , Z and L , respectively. In all models considered, we assume azimuthal symmetry about the Galactic center.

The spatial distribution of pulsars is rather loosely constrained, but we find that it does not affect the results significantly for a wide range of models. For the radial and the vertical PDFs, we consider Gaussian and exponential forms with different values of the radial R_0 and the vertical Z_0 scale. In our reference model, we assume a Gaussian PDF for the radial component and an exponential PDF for the vertical component. Hence, the combined spatial PDF is given by:

$$f(R, Z) \propto \exp\left(-\frac{R^2}{2R_0^2} - \frac{|Z|}{Z_0}\right), \quad (2)$$

We set $R_0 = 4.0$ kpc and $Z_0 = 1.5$ kpc as standard model parameters. Following Narayan et al. (1991), these and other values considered reflect the *present-day* spatial distribution of the NS–NS binary population after kinematic evolution in the Galactic gravitational potential.

Having assigned a position of each pulsar in our model galaxy, for later computational convenience, we store the positions as Cartesian x, y, z coordinates, where the Galactic center

is defined as (0.0,0.0,0.0) kpc and the position of the Earth is assumed to lie 8.5 kpc from the center along the $x - y$ plane, i.e. (8.5,0.0,0.0). From these definitions, the distance d to each pulsar from the Earth can be readily calculated, as well as the apparent Galactic coordinates l and b .

For the luminosity PDF, we follow the results of Cordes & Chernoff (1997) and adopt a power-law function of the form

$$\phi(L) = (p - 1)L_{\min}^{p-1}L^{-p}, \quad (3)$$

where $L \geq L_{\min}$ and $p > 1$. The cut-off luminosity, L_{\min} , and the exponent p are the model parameters. Cordes & Chernoff (1997) found $L_{\min} = 1.1_{-0.5}^{+0.4}$ mJy kpc 2 and $p = 2.0 \pm 0.2$ at 68% confidence. We set $p = 2.0$ and $L_{\min} = 1.0$ mJy kpc 2 for our reference model. Throughout this paper, luminosities are defined to be at the observing frequency $\nu = 400$ MHz.

Having defined the position and luminosity of each pulsar in our model Galaxy, the final step in defining the model population is to calculate a number of derived parameters required to characterize the detection of the model pulsars: dispersion measure (DM), scatter-broadening time (τ) and sky background temperature (T_{sky}). To calculate DM and τ , we use the software developed by Taylor & Cordes (1993) to integrate their model of the free-electron column density along the line of sight to each pulsar defined by its model Galactic coordinates l and b out to its distance d . Frequency scaling of τ to different survey frequencies is done assuming a Kolmogorov turbulence spectrum with a spectral index of -4.4 ¹. Finally, given the model Galactic coordinates of each pulsar, the sky background noise temperature at 408 MHz (T_{sky}) is taken from the all-sky catalog of Haslam et al. (1981). Scaling T_{sky} to other survey frequencies assumes a spectral index of -2.8 (Lawson et al. 1987).

4. PULSAR SURVEY SELECTION EFFECTS

Having created a model pulsar population with a given spatial and luminosity distribution, we are now in a position to determine the fraction of the total population which are actually *detectable* by current large-scale pulsar surveys. To do this, we need to calculate, for each model pulsar, the effective signal-to-noise ratio it would have in each survey and compare this with the corresponding detection threshold. Only those pulsars which are

¹Although recent studies suggest a variety of spectral indices for τ (Löhmer et al. 2001), the effects of scattering turn out to be negligible in this study since the detections of NS-NS binaries are limited by luminosity to nearby systems.

nominally above the threshold count as being detectable. After performing this process on the entire model pulsar population of size N_{tot} , we are left with a sample of N_{obs} pulsars that are nominally detectable by the surveys. Repeating this process many times, we can determine the probability distribution of N_{obs} which we then use to constrain the population and coalescence rate of NS–NS binaries. In this section we discuss our modeling of the various selection effects which limit pulsar detection.

4.1. Survey Parameters

The main factors affecting the signal-to-noise ratio (σ) of a pulsar search can be summarized by the following expression

$$\sigma \propto \frac{S_{\nu}G}{T} \sqrt{\frac{P\Delta\nu t}{w_e}}, \quad (4)$$

where S_{ν} is the apparent flux density at the survey frequency ν , G is the gain of the telescope, T is the effective system noise temperature (which includes a contribution T_{sky} from the sky background described in the previous section), P is the pulse period, $\Delta\nu$ is the observing bandwidth, t is the integration time and w_e is the pulse width. More exact expressions are given in the detailed description of the survey selection effects in §2 of LBDH (in particular see their eqns. 14–18) which we adopt in this work. In what follows, we describe the salient points relevant to this study.

For each model pulsar, with known 400-MHz luminosity L and distance d , we calculate the apparent 400-MHz flux density $S_{400} = L/d^2$. Since not all pulsar surveys are carried out at 400 MHz, we need to scale S_{400} to take account of the steep radio flux density spectra of pulsars. Using a simple power law of the form $S_{\nu} \propto \nu^{\alpha}$, where α is the spectral index, we can calculate the flux S_{ν} at any frequency ν as:

$$S_{\nu} = S_{400} \left(\frac{\nu}{400 \text{ MHz}} \right)^{\alpha}, \quad (5)$$

Following the results of Lorimer et al. (1995), in all simulations, spectral indices were drawn from a Gaussian PDF with a mean of -1.6 and standard deviation 0.4 .

The telescope gain, system noise, bandwidth and integration time are well-known parameters for any given survey and the detailed models we use take account of these. In addition to the surveys considered by LBDH, we also model surveys listed by Curran & Lorimer (1995), and more recent surveys at Green Bank (Sayer, Nice & Taylor 1997) and Parkes (Lyne et al. 2000; Manchester et al. 2001; Edwards et al. 2001). A complete list of the surveys considered, and the references to the relevant publications is given in Table 1.

Up to this point in the simulations, the model parameters are identical for both PSRs B1913+16 and B1534+12. Since we are interested in the individual contributions each of these systems make to the total Galactic merger rate of NS–NS binaries similar to these systems, we fix the assumed spin periods P and *intrinsic* pulse widths w to the values of each pulsar and perform separate simulations over all physical models considered. The assumed pulse widths are 10 ms and 1.5 ms respectively for PSRs B1913+16 and B1534+12. The *effective pulse width* w_e required for the signal-to-noise calculation must take into account pulse broadening effects due to the interstellar medium and the response of the observing system. The various contributions are summarized by the quadrature sum:

$$w_e^2 = w^2 + \tau^2 + t_{\text{samp}}^2 + t_{\text{DM}}^2 + t_{\Delta\text{DM}}^2, \quad (6)$$

where τ is the scatter-broadening timescale calculated from the Taylor & Cordes (1993) model, t_{samp} is the data sampling interval in the observing system, t_{DM} is the dispersive broadening across an individual frequency channel and $t_{\Delta\text{DM}}$ is the pulse broadening due to dedispersion at a slightly incorrect dispersion measure. All of these factors are accounted for in our model described in detail in LBDH.

4.2. Doppler Smearing

For binary pulsars, we need to take account of the reduction in signal-to-noise ratio due to the Doppler shift in period during an observation. This was not considered in LBDH since their analysis was concerned only with isolated pulsars. For observations of NS–NS binaries, however, where the orbital periods are of the order of 10 hours or less, the apparent pulse period can change significantly during a search observation causing the received power to be spread over a number of frequency bins in the Fourier domain. As all the surveys considered in this analysis search for periodicities in the amplitude spectrum of the Fourier transform of the time series, a signal spread over several bins can result in a loss of signal-to-noise ratio. To take account of this effect in our survey simulations, we need to multiply the apparent flux density of each model pulsar by a “degradation factor”, F .

To calculate the appropriate F values to use, we generate synthetic pulsar search data containing signals with periods and duty cycles similar to PSR B1913+16 and PSR B1534+12. These data are then passed through a real pulsar search code which is similar to those in use in the large-scale surveys (see Lorimer et al. 2000 for details). For each of the two pulsars, we first generate a control time series in which the signal has a constant period and find the resulting signal-to-noise ratio, σ_{control} , reported by the search code. We then generate a time series in which the pulses have identical intensity but are modulated in period according to the appropriate orbital parameters of each binary pulsar. From the resulting

search signal-to-noise ratio, σ_{binary} , the degradation factor $F = \sigma_{\text{binary}}/\sigma_{\text{control}}$. Significant degradation occurs, therefore, when $F \ll 1$. Since accumulated Doppler shift, and therefore F , is a strong function of the orbital phase at the start of a given observation, for both binary systems, we calculate the mean value of F for a variety of starting orbital phases appropriately weighted by the time spent in that particular part of the orbit.

A similar analysis was made by Camilo et al. (2000) for the millisecond pulsars in 47 Tucanae. In this paper, where we are interested in the degradation as a function of integration time, we generate time series with a variety of lengths between 1 minute and 1 hour using sampling intervals similar to those of the actual surveys listed in Table 1. The results are summarized in Figure 1, where we plot average F versus integration time for both sets of orbital parameters. As expected, surveys with the longest integration times are most affected by Doppler smearing. For the Parkes Multibeam survey (Lyne et al. 2000; Manchester et al. 2001), which has an integration time of 35 min, mean values of F are 0.7 and 0.3 for PSR B1913+16 and PSR B1534+12 respectively². The greater degradation for PSR B1534+12 is due to its mildly eccentric orbit ($e \sim 0.3$ versus 0.6 for PSR B1913+16) which results in a much more persistent change in apparent pulse period when averaged over the entire orbit. For the Jodrell Bank and Swinburne surveys (Nicastro et al. 1995; Edwards et al. 2001), which both have integration times of order 5 min, we find $F \sim 0.9$ for both systems. For all other surveys, which have significantly shorter integration times, no significant degradation is seen, and we take $F = 1$.

5. STATISTICAL ANALYSIS

In this section we describe in detail the derivation of the probability distribution of the Galactic coalescence rate \mathcal{R} . The analysis method makes use of Bayesian statistics and takes into account the rate contributions of both observed NS–NS binaries. At the end of the section we derive the associated detection rates for LIGO.

²In order to improve on the sensitivity to binary pulsars, the Parkes Multibeam survey data are now being reprocessed using various algorithms designed to account for binary motion during the integration time (Faulkner et al. 2002)

5.1. The Rate Probability Distribution for Each Observed NS–NS Binary

As already mentioned in § 2, for each of the two observed NS–NS binaries (PSR B1913+16 or PSR B1534+12) we generate pulsar populations in physical and radio luminosity space with pulse periods and widths fixed to the observed ones and with different absolute normalizations, i.e., total number N_{tot} of pulsars in the Galaxy. We generate large numbers of “observed” pulsar samples by modeling the pulsar survey selection effects (see § 4) and applying them on these model populations of PSR B1913+16–like and PSR B1534+12–like pulsars separately (see § 3). For a fixed value of N_{tot} , we use these “observed” samples to calculate the distribution of the number of objects in the samples. One might expect that the number of observed pulsars in a sample N_{obs} follows very closely a Poisson distribution:

$$P(N_{\text{obs}}; \lambda) = \frac{\lambda^{N_{\text{obs}}} e^{-\lambda}}{N_{\text{obs}}!}, \quad (7)$$

where, by definition, $\lambda \equiv \langle N_{\text{obs}} \rangle$. We confirm our expectation by obtaining excellent formal fits to the Monte Carlo data using such a distribution and calculating the best-fitting value of λ . We vary N_{tot} in the range $10 - 10^4$ and find that λ is linearly correlated with N_{tot} :

$$\lambda = \alpha N_{\text{tot}}, \quad (8)$$

where α is a constant that depends on the properties (space and luminosity distributions and pulse period and width) of the Galactic pulsar population. Examples of the Poisson fits and the linear correlations are shown in Figures 2 and 3, respectively, for our reference model 1 (see Table 2 and § 6).

The main step in deriving a rate probability distribution for each of the observed systems is to first derive the probability distribution of the total number of pulsars like the observed ones in the Galaxy. We obtain the latter by applying Bayes’ theorem:

$$P(H|DX) = P(H|X) \frac{P(D|HX)}{P(D|X)}, \quad (9)$$

where $P(H|DX)$ is the probability of a model hypothesis H given data D and model priors X , $P(D|HX)$ is the likelihood of the data given a model hypothesis and priors, $P(H|X)$ is the probability of a model hypothesis in the absence of any data information, and $P(D|X)$ is the model prior probability, which acts as a normalization constant.

In the present work, we make following identifications:

D : is the real observed sample

H : is λ proportional to N_{tot}

X : is the population model (space and luminosity distributions and pulse period and width)

With these identifications, $P(D|HX)$ is the likelihood of the real observed sample (one “PSR B1913+16-like” and one “PSR B1534+12-like” pulsar) and is obtained by the best-fitting Poisson distribution:

$$P(D|HX) = P(1; \lambda(N_{\text{tot}}), X) = \lambda(N_{\text{tot}}) e^{-\lambda(N_{\text{tot}})}. \quad (10)$$

In the absence of any data information, the absolute normalization of the model population, i.e., the total pulsar number N_{tot} and hence λ is expected to be *independent* of the shape of the population distributions and properties represented by X . Therefore, the probability of λ given a set of assumptions X for the model Galactic population is expected to be flat:

$$P(H|X) = P(\lambda(N_{\text{tot}})|X) = \text{constant}, \quad (11)$$

and is essentially absorbed by the model prior probability $P(D|X)$ as a normalization constant. The probability distribution of λ then is given by:

$$P(\lambda|DX) = \frac{P(\lambda|X)}{P(D|X)} P(1; \lambda, X) = \text{constant} \times P(1; \lambda, X). \quad (12)$$

We impose the normalization constraint: $\int_0^\infty P(\lambda|DX)d\lambda = 1$ and find that $P(H|X)/P(D|X) = 1$ and

$$P(\lambda|DX) = P(1; \lambda, X) = \lambda e^{-\lambda}. \quad (13)$$

Note that based on the above expression, the maximum value of $P(\lambda)$ equal to e^{-1} always occurs at $\lambda = 1$ or at $N_{\text{tot}} = \alpha^{-1}$ (see eq.(8)). It is straightforward to calculate $P(N_{\text{tot}})$:

$$\begin{aligned} P(N_{\text{tot}}) &= P(\lambda) \left| \frac{d\lambda}{dN_{\text{tot}}} \right| \\ &= \alpha^2 N_{\text{tot}} e^{-\alpha N_{\text{tot}}} \end{aligned} \quad (14)$$

For a given total number of pulsars in the Galaxy, we can calculate their rate using estimates of the associated pulsar beaming correction factor f_b and lifetime τ_{life} :

$$\mathcal{R} = \frac{N_{\text{tot}}}{\tau_{\text{life}}} f_b. \quad (15)$$

Note that this estimate is equivalent to previous studies (KNST and references therein) where the concept of the *scale factor* is used instead of our calculated N_{tot} . We can write equivalently for our calculation:

$$\frac{N_{\text{tot}}}{N_{\text{obs}}} = \frac{\int \int_{V_G} f(R, Z, L) dV dL}{\int \int_{V_D} f(R, Z, L) dV dL}, \quad (16)$$

where $f(R, Z, L)$ is the probability distribution of the pulsar population (§ 3), V_G and V_D are the Galactic volume and the detection volume (for pulsars with pulse period and width similar to each of the two observed pulsars), respectively. Note that we do not fix the luminosity of the pulsar population to the observed values, but instead, we estimate N_{tot} for a distribution of radio luminosities. Since we consider separately PSR B1913+16-like and PSR B1534+12-like populations, $N_{\text{obs}} = 1$.

For pulsar beaming fractions, we adopt the estimates obtained by KNST: 5.72 for PSR B1913+16 and 6.45 for PSR B1534+12. For the lifetime estimates we also follow KNST. Our adopted values for the pulsar lifetimes are 3.65×10^8 yr for PSR B1913+16 and 2.9×10^9 yr for PSR B1534+12.

Using eq. (15) we calculate $P(\mathcal{R})$ for each of the two observed pulsars:

$$\begin{aligned} P(\mathcal{R}) &= P(N_{\text{tot}}) \left| \frac{dN_{\text{tot}}}{d\mathcal{R}} \right| \\ &= \left(\frac{\alpha \tau_{\text{life}}}{f_b} \right)^2 \mathcal{R} e^{-\left(\frac{\alpha \tau_{\text{life}}}{f_b} \right) \mathcal{R}}. \end{aligned} \quad (17)$$

5.2. The Total Galactic Coalescence Rate

Once the probability distributions of the rate contributions of the two observed pulsars are calculated, we can obtain the distribution functions of the total coalescence rate \mathcal{R}_{tot} . We define the following two coefficients for each observed system:

$$A \equiv \left(\frac{\alpha \tau_{\text{life}}}{f_b} \right)_{1913} \quad \text{and} \quad B \equiv \left(\frac{\alpha \tau_{\text{life}}}{f_b} \right)_{1534} \quad (18)$$

and rewrite the coalescence rate for each binary system:

$$P_{1913}(\mathcal{R}) = A^2 \mathcal{R} e^{-A\mathcal{R}} \quad \text{and} \quad P_{1534}(\mathcal{R}) = B^2 \mathcal{R} e^{-B\mathcal{R}}. \quad (19)$$

One can confirm that each distribution function satisfies the normalization condition

$$\int_0^\infty P(\mathcal{R}) d\mathcal{R} = 1. \quad (20)$$

We then define two new variables: $\mathcal{R}_+ \equiv \mathcal{R}_{1913} + \mathcal{R}_{1534}$ and $\mathcal{R}_- \equiv \mathcal{R}_{1913} - \mathcal{R}_{1534}$. Since $\mathcal{R}_{1913} \geq 0$ and $\mathcal{R}_{1534} \geq 0$, we have $-\mathcal{R}_+ \leq \mathcal{R}_- \leq \mathcal{R}_+$. For convenience, we rename $\mathcal{R}_{1913} = \mathcal{R}_1$ and $\mathcal{R}_{1534} = \mathcal{R}_2$ and perform a two-dimensional probability distribution transformation:

$$P(\mathcal{R}_+, \mathcal{R}_-) = P(\mathcal{R}_1, \mathcal{R}_2) \begin{vmatrix} \frac{d\mathcal{R}_1}{d\mathcal{R}_+} & \frac{d\mathcal{R}_2}{d\mathcal{R}_-} \\ \frac{d\mathcal{R}_1}{d\mathcal{R}_-} & \frac{d\mathcal{R}_2}{d\mathcal{R}_+} \end{vmatrix} = \frac{1}{2} P(\mathcal{R}_1, \mathcal{R}_2). \quad (21)$$

The probability distribution of the total rate $\mathcal{R}_{\text{tot}} \equiv \mathcal{R}_+$ is obtained after integrating $P(\mathcal{R}_+, \mathcal{R}_-)$ over \mathcal{R}_- :

$$P(\mathcal{R}_+) = \int_{\mathcal{R}_-} P(\mathcal{R}_+, \mathcal{R}_-) d\mathcal{R}_- = \frac{1}{2} \int_{\mathcal{R}_-} P(\mathcal{R}_1, \mathcal{R}_2) d\mathcal{R}_-. \quad (22)$$

Since the probability distributions for the rate contributions of each of the two observed pulsars are independent of each other, their two-dimensional distribution is simply the product of the two.

$$P(\mathcal{R}_1, \mathcal{R}_2) = P(\mathcal{R}_1)P(\mathcal{R}_2). \quad (23)$$

After we replace all variables to \mathcal{R}_+ and \mathcal{R}_- , we have

$$\begin{aligned} P(\mathcal{R}_+ \equiv \mathcal{R}_{\text{tot}}) &= \frac{A^2 B^2}{2^3} e^{-(\frac{A+B}{2})\mathcal{R}_+} \left[\mathcal{R}_+^2 \int_{-\mathcal{R}_+}^{+\mathcal{R}_+} d\mathcal{R}_- e^{(\frac{B-A}{2})\mathcal{R}_-} - \int_{-\mathcal{R}_+}^{+\mathcal{R}_+} d\mathcal{R}_- \mathcal{R}_-^2 e^{(\frac{B-A}{2})\mathcal{R}_-} \right] \\ &= \left(\frac{AB}{B-A} \right)^2 \left[\mathcal{R}_+ (e^{-A\mathcal{R}_+} + e^{-B\mathcal{R}_+}) - \left(\frac{2}{B-A} \right) (e^{-A\mathcal{R}_+} - e^{-B\mathcal{R}_+}) \right]. \end{aligned} \quad (24)$$

We have confirmed that the above function satisfies the normalization $\int_0^\infty P(\mathcal{R}_{\text{tot}}) d\mathcal{R}_{\text{tot}} = 1$.

Having calculated the probability distribution of the Galactic coalescence rate, we can take one step further and also calculate ranges of values for the rate \mathcal{R}_{tot} at various confidence levels (CL). The lower (\mathcal{R}_a) and upper (\mathcal{R}_b) limits to these ranges are calculated using:

$$\int_{\mathcal{R}_a}^{\mathcal{R}_b} P(\mathcal{R}_{\text{tot}}) d\mathcal{R}_{\text{tot}} = \text{CL} \quad (25)$$

and

$$P(\mathcal{R}_a) = P(\mathcal{R}_b). \quad (26)$$

In all our results, we quote coalescence rates for 68%, 95% and 99% CL.

5.3. The Detection Rate for LIGO

NS-NS binary systems are expected to emit strong gravitational waves during their inspiral phase, the late stages of which may be detected by the ground-based gravitational wave detectors. In this paper we estimate expected detection rates for LIGO (initial and advanced) using the derived probability distribution of the Galactic rate and its values at the maximum of the distribution, for different physical models of pulsar properties. To calculate the detection rate, we need to extrapolate the Galactic rate to the volume detectable by LIGO. We use the ratio between the B-band luminosity density of the Universe and the B-band luminosity of our Galaxy as the scaling factor (Phinney 1991; KNST). This is based

on the assumptions that (i) the B-band luminosity (corrected for dust absorption) correlates with the star-formation rate in the nearby universe and hence the coalescence rate, (ii) the B-band luminosity density is constant in the nearby universe. The detection rate, \mathcal{R}_{det} , is calculated by the following equation:

$$\mathcal{R}_{\text{det}} = \epsilon \mathcal{R}_{\text{tot}} V_{\text{det}}, \quad (27)$$

where ϵ is the scaling factor assumed to be $\simeq 10^{-2} \text{ Mpc}^{-3}$ (for details see KNST). V_{det} is the detection volume defined as a sphere with a radius equals to the maximum detection distance D_{max} for the initial ($\simeq 20 \text{ Mpc}$) and advanced LIGO ($\simeq 350 \text{ Mpc}$) (Finn 2001).

6. RESULTS

We have calculated the probability distribution of the Galactic coalescence rate \mathcal{R}_{tot} , its most likely value $\mathcal{R}_{\text{peak}}$ and ranges at different statistical confidence levels, and the most likely expected detection rates for the initial and advanced LIGO for a large number of model pulsar population properties (see Table 2). We have chosen one of them to be our *reference* model based on the statistical analyses and results presented by Cordes & Chernoff (1997).

For our reference model ($L_{\text{min}} = 1.0 \text{ mJy kpc}^2$, $p = 2.0$, $R_{\text{o}} = 4.0 \text{ kpc}$, and $Z_0 = 1.5 \text{ kpc}$), we find the most likely value of N_{tot} , to be $\simeq 390$ pulsars for the “PSR B1913+16-like” population, and $\simeq 350$ pulsars for the “PSR B1534+12-like” population. Using eq. (24), we evaluate the total Galactic coalescence rate of NS-NS binaries for this reference case (model 1 in Table 2). The most likely value of the coalescence rate is $\simeq 8 \text{ Myr}^{-1}$ and the ranges at different statistical confidence levels are: $\sim 3 - 20 \text{ Myr}^{-1}$ at 68%, $\sim 1 - 30 \text{ Myr}^{-1}$ at 95%, and $\sim 0.7 - 40 \text{ Myr}^{-1}$ at 99%.

In Figure 4, $P(\mathcal{R}_{\text{tot}})$ along with $P(\mathcal{R}_{1913})$ and $P(\mathcal{R}_{1534})$ are shown for the reference model. It is evident that the total rate distribution is dominated by that of PSR B1913+16. At first this appears to be in contradiction to most other studies of the NS-NS coalescence rate (Narayan et al. 1991; Phinney 1991; Curran & Lorimer 1995; van den Heuvel & Lorimer 1996; Stairs et al. 1998; Arzoumanian et al. 1999; KNST). However, it turns out that this difference is due to the fact that earlier studies restricted the scale factor calculation to the actual observed pulsar luminosity and the rate estimates were dominated by the low luminosity of and hence large scale factor for PSR B1534+12. Any corrections to the rate estimate because of a range of pulsar luminosities were applied as subsequent upward corrections. However, this effect is eliminated in our case because we calculate the two rate contributions having relaxed the luminosity constraint and instead having allowed

for a range in luminosity for the pulsars. In this case any differences in the two separate rate contributions depend *only* on differences in pulse periods, and widths. Given that the latter are rather small, it makes sense that, for example, the most likely values of N_{tot} for the two pulsars come out to be very similar (e.g. $\simeq 390$ and $\simeq 350$, for PSR B1913+16 and PSR B1534+12, respectively, in model 1). Consequently any difference in the rate contributions from the two populations is due to the difference in lifetimes (about a factor of 10) for the two observed pulsars (note that the two do not only have similar N_{tot} estimates, but also similar beaming correction factors). Since the lifetime estimate for PSR B1913+16 is much smaller, the total rate distribution is dominated by its contribution.

In Table 2 we list the population parameters and results of Galactic coalescence and LIGO detection rates for a large number of models (but still a subset of the models we have investigated in detail). Model 1 is our reference model defined above and the rest of the models are used to explore the sensitivity of our results on the pulsar population properties in luminosity and space distributions. The variation of the luminosity function parameters is within ranges that correspond to 68% confidence levels from the statistical analysis of Cordes & Chernoff (1997). The variation of the space scale lengths R_0 and Z_0 extends to values that are not favored by our current understanding, only to allow us to examine the presence of any correlations. Scrutiny of the results presented in Table 2 reveals that rate estimates are modestly sensitive (and in some cases, e.g., Z_0 , insensitive) to most of these variations, except in cases of very low values of L_{min} , down to 0.3 mJy kpc², and unphysically low values of R_0 , down to 2–3 kpc. Assumptions about the shape of the space distribution (exponential or Gaussian) are not important. The most important model parameter seems to be the slope of the luminosity function. The most likely values for the rates are found in the range $\simeq 3$ –22 Myr^{−1} for all models with luminosity-function parameters consistent with a 68% confidence level estimated by Cordes & Chernoff (1997) and R_0 in the range 4–8 kpc. Within a given model the range of estimated values at 68% confidence level is typically broad by a factor of 5, while at the 95% level the ranges broaden by another factor of about 5, reaching an uncertainty of ~ 25 for the rate estimates.

In terms of qualitative variations, it is clear that models with increasing fraction of low-luminosity or very distant pulsars lead to increasing rate estimates, as expected. A demonstration of this kind of dependence is shown in Figures 5 and 6. We have found that there is a strong correlation between the peak value of the total Galactic coalescence rate $\mathcal{R}_{\text{peak}}$ estimated by eq. (24) and the cut-off luminosity L_{min} and the power index p . As seen in these Figures $\mathcal{R}_{\text{peak}}$ increases rapidly with decreasing L_{min} (Fig. 5) or with increasing p (Fig. 6). Scale lengths of the spatial distribution (either R_0 or Z_0) do not show a correlation with $\mathcal{R}_{\text{peak}}$ as strong as that of the luminosity-function parameters. In Figure 7 the most likely rate estimate is plotted as a function of the radial scale length R_0 . It is evident that the

rate is relatively insensitive to R_0 variations unless its values becomes very small ($\lesssim 3$ kpc). Small values of the radial scale for the Galactic distribution implies a large fraction of very distant (and hence undetectable) pulsars in the Galaxy and leads to a rapid increase of the estimated coalescence rate. However, such small R_0 values are not consistent with our current understanding of stellar populations in the Galaxy (Lyen et al. 1985).

7. DISCUSSION

In this paper we present a new method of estimating the total number of pulsars in our Galaxy and we apply it to the calculation of the coalescence rate of double neutron star systems in the Galactic field. The method implicitly takes into account the small number of pulsars in the observed double-neutron-star sample as well as their distribution in luminosity and space in the Galaxy. The modeling of pulsar survey selection effects is formulated in a “forward” way, by populating the Galaxy with model pulsar populations and calculating the likelihood of the real observed sample. This is in contrast to the “inverse” way of the calculation of scale factors used in previous studies. The formulation presented here allows us to: (a) calculate the probability distribution of coalescence rates; (b) assign statistical significance to these estimates; and (c) and quantify the uncertainties associated with them.

As originally shown by KNST, the most important uncertainties originate from the combination of a small-number observed pulsar and a pulsar population dominated by faint objects. The probability distribution covers more than 2 orders of magnitude in agreement with the uncertainties in excess of two orders of magnitudes asserted by KNST. However, even at high statistical confidence level (99%) the uncertainty is reduced to a factor of ~ 60 . At confidence levels of 95% and 68%, the uncertainty is further reduced to just ~ 25 and ~ 5 , respectively. We use our results to estimate the expected detection rates for ground-based interferometers, such as LIGO. The most likely values are found in the range $\sim (1 - 30) \times 10^{-3} \text{ yr}^{-1}$ and $\sim 4 - 100 \text{ yr}^{-1}$, for the initial and advanced LIGO.

The statistical method developed here can be further extended to account for distributions of pulsar populations in pulse periods, widths, and orbital periods. Most importantly the method can be applied to any type of pulsar population with appropriate modifications of the modeling of survey selection effects. Currently we are working on assessing the contribution of double neutron stars formed in globular clusters as well as the formation rate of binary pulsars with white dwarf companions that are important for gravitational-wave detection by LISA, the space-based interferometer planned by NASA and ESA for the end of this decade.

This work is partially supported by NSF grant PHY-0121420 to VK. DRL is a University Research Fellow funded by the Royal Society. DRL is also grateful for the hospitality and support of the Theoretical Astrophysics Group at Northwestern U. VK would also like to acknowledge partial support by the Clay Fellowship at the Smithsonian Astrophysical Observatory where this work was initiated.

REFERENCES

Arzoumanian, Z., Cordes, J. M. & Wasserman, I. 1999 *ApJ*, 520, 696

Belczynski, K. & Kalogera, V. 2001, *ApJ*, 550, L183

Camilo, F., Nice, D. J., Sharuner, J. & Taylor, J. H. 1996, *ApJ*, 469, 819

Camilo, F., Lorimer, D. R., Freire, P., Lyne, A. G. & Manchester, R. N. 2000 *ApJ*, 535, 975

Clark, J. P. A., van den Heuvel, E. P. J. & Sutantyo, W. 1979, *A&A*, 72, 120

Clifton, T. R., Lyne, A. G., Jones, A. W., McKenna, J. & Ashworth, M. 1992, *MNRAS*, 254, 177

Cordes, J. M., & Chernoff D. F. 1997, *ApJ*, 482, 971

Curran, S. J. & Lorimer, D. R. 1995, *MNRAS*, 276, 347

D'Amico, N., Manchester, R. N., Durdin, J. M., Stokes, G. H., Stinebring, D. R., Taylor, J. H. & Brissenden, R. J. V. 1988, *MNRAS*, 234, 437

Damashek, M., Backus, P. R., Taylor, J. H. & Burkhardt, R. K. 1982, *ApJ*, 253, L57

Damashek, M., Taylor, J. H. & Hulse, R. A. 1978, *ApJ*, 225, L31

Davies, J. G., Lyne, A. G. & Seiradakis, J. H. 1972, *Nature*, 240, 229

Davies, J. G., Lyne, A. G. & Seiradakis, J. H. 1973, *Nature*, 244, 84

Dewey, R. J., Taylor, J. H., Weisberg, J. M. & Stokes, G. H. 1985, *ApJ*, 294, L25

Edwards, R. T., Bailes, M., van Straten, W. & Britton, M. 2001 *MNRAS*, 326, 358

Faulkner, A. J. et al. 2002, in: “Radio Pulsars” Eds: Bailes, M., Thorsett, S. E. & Nice, D. J., *PASP*, in press

Finn, L. S. 2001, *AIP conf. proceedings*, 575, 92

Foster, R. S., Cadwell, B. J., Wolszczan, A. & Anderson, S. B. 1995, *ApJ*, 454, 826

Haslam, C. G. T., Stoffel, H., Salter, C. J. & Wilson, W. E. 1982, *A&AS*, 47, 1

Hulse, R. A. & Taylor, J. H. 1974, *ApJ*, 191, L61

Hulse, R. A. & Taylor, J. H. 1975, *ApJ*, 195, L51

Johnston, S., Lyne, A. G., Manchester, R. N., Kniffen, D. A., D'Amico, N., Lim, J. & Ashworth, M. 1992, *MNRAS*, 255, 401

Johnston, H. M. & Kulkarni, S. R. 1991, *ApJ*, 368, 504

Kalogera, V., Narayan, R., Spergel, D. N. & Taylor J. H. 2001, *ApJ*, 556, 340 (KNST)

Lawson, K. D., Mayer, C. J., Osborne, J. L. & Parkinson, M. L. 1987, *MNRAS*, 225, 307

Löhmer, O., Kramer, M., Mitra, D., Lorimer, D. R. & Lyne, A. G. 2001, *ApJ*, 562, L157

Lorimer, D. R., Bailes, M., Dewey, R. J. & Harrison, P. A. 1993, *MNRAS*, 263, 403 (LBDH)

Lorimer, D. R., Yates, J. A., Lyne, A. G. & Gould, D. M. 1995, *MNRAS*, 273, 411

Lundgren, S. C., Zepka, A. F. & Cordes, J. M. 1995, *ApJ*, 453, 419

Lyne, A. G., Manchester, R. N. & Taylor, J. H. 1985, *MNRAS*, 213, 613

Lyne, A. G., et al. 1998, *MNRAS*, 295, 743

Lyne, A. G., et al. 2000, *MNRAS*, 312, 698

Manchester, R. N., Lyne, A. G., Taylor, J. H., Durdin, J. M., Large, M. I. & Little, A. G. 1978, *MNRAS*, 185, 409

Manchester, R. N., et al. 1996, *MNRAS*, 279, 1235

Manchester, R. N., et al. 2001, *MNRAS*, 328, 17

Narayan, R. 1987, *ApJ*, 319 162

Narayan, R., Piran, T. & Shemi, A. 1991, *ApJ*, 379, L17

Nicastro, L., Lyne, A. G., Lorimer, D. R., Harrison, P. A., Bailes, M. & Skidmore, B. D. 1995, *MNRAS*, 273, L68

Nice, D. J., Fruchter, A. S. & Taylor, J. H. 1995, *ApJ*, 449, 156

Phinney, E. S. 1991, *ApJ*, 380, L17

Popham, R., Woosley, S. E. & Fryer, C. 1998, *ApJ*, 518, 356

Prince, T. A., Anderson, S. B., Kulkarni, S. R. & Wolszczan, A. 1991, *ApJ*, 374, L41

Ray, P. S., Thorsett, S. E., Jenet, F. A., van Kerkwijk, M. H., Kulkarni, S. R., Prince, T. A., Sandhu, J. S. & Nice, D. J. 1996, *ApJ*, 470, 1103

Sayer, R. W., Nice, D. J. & Taylor, J. H. 1997, *ApJ*, 474, 426

Stairs, I. H., Arzoumanian, Z., Camilo, F., Lyne, A. G., Nice, D. J., Taylor, J. H., Thorsett, S. E., & Wolszczan, A. 1998, *ApJ*, 505, 352

Stokes, G. H., Segelstein, D. J., Taylor, J. H. & Dewey, R. J. 1986, *ApJ*, 311, 694

Taylor, J. H. & Cordes, J. M. 1993, *ApJ*, 411, 674

Taylor, J. H., Fowler, L. A. & McCulloch, P. M. 1979, *Nature*, 277, 437

Taylor, J. H. & Weisberg, J. M. 1982, *ApJ*, 253, 908

van den Heuvel, E. P. J. & Lorimer, D. R. 1996, *MNRAS*, 283, L37

Wolszczan, A. 1991, *Nature*, 350, 688

Table 1. Simulated Pulsar Surveys

Telescope	Year	ν^1	$\Delta\nu^2$	t_{obs}^3	t_{samp}^4	S_{min}^5	Detected ⁶	Refs ⁷
Lovell 76 m	1972	408	4	660	40	10	51/31	1,2
Arecibo 305 m	1974	430	8	137	17	1	50/40	3,4
Molonglo	1977	408	4	45	20	10	224/155	5
Green Bank 300'	1977	400	16	138	17	10	50/23	6,7
Green Bank 300'	1982	390	16	138	17	2	83/34	8
Green Bank 300'	1983	390	8	132	2	5	87/20	9
Lovell 76 m	1983	1400	40	524	2	1	61/40	10
Arecibo 305 m	1984	430	1	40	0.3	3	24/5	9
Molonglo	1985	843	3	132	0.5	8	10/1	11
Arecibo 305 m	1987	430	10	68	0.5	1	61/24	12
Parkes 64 m	1988	1520	320	150	0.3	1	100/46	13
Arecibo 305 m	1990	430	10	40	0.5	2	2/2	14
Parkes 64 m	1992	430	32	168	0.3	3	298/101	15,16
Arecibo 305 m	1993	430	10	40	0.5	1	56/90	17–20
Lovell 76 m	1994	411	8	315	0.3	5	5/1	21
Green Bank 140'	1995	370	40	134	0.3	8	84/8	22
Parkes 64 m	1998	1374	288	265	0.1	0.5	69/170	23
Parkes 64 m	1998	1374	288	2100	0.3	0.2	~900/600	24,25

¹Center frequency in MHz.

²Bandwidth in MHz.

³Integration time in seconds.

⁴Sampling time in milliseconds.

⁵Sensitivity limit in mJy at the survey frequency for long-period pulsars (calculated for each trial in the simulations).

⁶Total number of detections and new pulsars

⁷ References: (1,2) Davies, Lyne & Seiradakis (1972,3); (3,4) Hulse & Taylor (1974,5); (5) Manchester et al. (1978); (6,7) Damashek et al. (1978,1982); (8) Dewey et al. (1985); (9) Stokes et al. (1986); (10) Clifton et al. (1992); (11) D'Amico et al. (1988); (12) Nice, Taylor & Fruchter (1995); (13) Johnston et al. (1992); (14) Wolszczan (1991); (15) Manchester et al. (1996); (16) Lyne et al. (1998); (17) Ray et al. (1996); (18) Camilo et al. (1996); (19) Foster et al. (1995); (20) Lundgren, Zepka & Cordes (1995); (21) Nicastro et al. (1995); (22) Sayer, Nice & Taylor (1997); (23) Edwards et al. (2001); (24) Lyne et al. (2000); (25) Manchester et al. (2002)

Table 2. Model Parameters and Estimates for \mathcal{R}_{tot} and \mathcal{R}_{det} at Various Statistical Confidence Levels for Different Population Models

Model ¹	Parameters				\mathcal{R}_{tot} (Myr ⁻¹)			\mathcal{R}_{det} of LIGO (yr ⁻¹)			
	L_{min}^2 (mJy kpc ²)	p^3	R_0^4 (kpc)	Z_0^5 (kpc)	peak ⁷	68% ⁸	95% ⁸	initial peak ⁷	$\times 10^{-3}$ 68% ⁸	advanced peak ⁷	68% ⁸
1	1.0	2.0	4.0 (G ⁶)	1.5 (E ⁶)	8.0	+9.3 -4.7	+23.3 -6.7	3.3	+3.9 -2.0	17.9	+21.0 -10.6
2	1.0	2.0	4.0 (G)	0.5 (E)	7.1	+8.3 -4.2	+20.8 -5.9	3.0	+3.5 -1.7	15.9	+18.7 -9.4
3	1.0	2.0	4.0 (G)	2.0 (E)	8.4	+9.9 -5.0	+24.7 -7.1	3.5	+4.1 -2.1	19.0	+22.2 -11.2
4	1.0	2.0	4.0 (E)	1.5 (E)	8.7	+10.2 -5.1	+25.6 -7.3	3.6	+4.3 -2.2	19.5	+23.0 -11.6
5	1.0	2.0	4.0 (G)	1.5 (G)	7.9	+9.2 -4.6	+23.0 -6.6	3.3	+3.9 -1.9	17.7	+20.7 -10.
6	0.3	2.0	4.0 (G)	1.5 (E)	26.9	+32.0 -16.1	+80.3 -22.7	11.3	+13.4 -6.7	60.5	+72.1 -36.2
7	0.7	2.0	4.0 (G)	1.5 (E)	11.5	+13.5 -6.8	+33.9 -9.7	4.8	+5.7 -2.9	25.9	+30.5 -15.3
8	1.5	2.0	4.0 (G)	1.5 (E)	5.5	+6.3 -3.2	+15.9 -4.6	2.3	+2.7 -1.3	12.3	+14.3 -7.2
9	3.0	2.0	4.0 (G)	1.5 (E)	3.4	+4.2 -2.1	+10.4 -2.9	1.4	+1.7 -0.9	7.7	+9.3 -4.6
10	0.3	1.8	4.0 (G)	1.5 (E)	9.4	+10.8 -5.5	+27.1 -7.9	3.9	+4.5 -2.3	21.2	+24.3 -12.4
11	0.7	1.8	4.0 (G)	1.5 (E)	4.8	+5.4 -2.8	+13.5 -4.0	2.0	+2.3 -1.2	10.7	+12.2 -6.2
12	1.0	1.8	4.0 (G)	1.5 (E)	3.6	+4.1 -2.1	+10.3 -3.0	1.5	+1.7 -0.9	8.2	+9.3 -4.7
13	1.5	1.8	4.0 (G)	1.5 (E)	2.7	+3.0 -1.5	+7.6 -2.2	1.1	+1.3 -0.6	6.0	+6.8 -3.5
14	3.0	1.8	4.0 (G)	1.5 (E)	1.6	+1.8 -0.9	+4.4 -1.3	0.7	+0.7 -0.4	3.5	+4.0 -2.0
15	0.3	2.2	4.0 (G)	1.5 (E)	61.2	+75.8 -37.5	+190.3 -52.1	25.6	+31.7 -15.7	137.6	+170.5 -84.4
16	0.7	2.2	4.0 (G)	1.5 (E)	22.1	+27.0 -13.4	+67.8 -18.7	9.2	+11.3 -5.6	49.7	+60.8 -30.2
17	1.0	2.2	4.0 (G)	1.5 (E)	14.9	+18.0 -9.0	+45.2 -12.6	6.2	+7.5 -3.8	33.5	+40.5 -20.2
18	1.5	2.2	4.0 (G)	1.5 (E)	9.8	+11.7 -5.9	+29.4 -8.2	4.1	+4.9 -2.5	22.0	+26.4 -13.2
19	3.0	2.2	4.0 (G)	1.5 (E)	4.7	+5.5 -2.8	+13.8 -3.9	2.0	+2.3 -1.2	10.5	+12.4 -6.2
20	1.0	2.5	4.0 (G)	1.5 (E)	28.3	+35.6 -17.5	+89.4 -24.2	11.8	+14.9 -7.3	63.6	+80.0 -39.4
21	1.0	2.0	2.0 (G)	1.5 (E)	26.1	+29.7 -15.2	+74.2 -21.7	10.9	+12.4 -6.3	58.6	+66.7 -34.1
22	1.0	2.0	3.0 (G)	1.5 (E)	12.8	+14.6 -7.4	+36.4 -10.7	5.4	+6.1 -3.1	28.9	+32.8 -16.8
23	1.0	2.0	5.0 (G)	1.5 (E)	6.7	+7.9 -4.0	+19.8 -5.6	2.8	+3.3 -1.7	15.1	+17.8 -8.9
24	1.0	2.0	6.0 (G)	1.5 (E)	6.6	+7.8 -3.9	+19.5 -5.5	2.7	+3.3 -1.6	14.8	+17.5 -8.8
25	1.0	2.0	7.0 (G)	1.5 (E)	6.9	+8.2 -4.1	+20.5 -5.8	2.9	+3.4 -1.7	15.5	+18.4 -9.2
26	1.0	2.0	8.0 (G)	1.5 (E)	7.4	+8.8 -4.4	+22.2 -6.3	3.1	+3.7 -1.9	16.8	+19.9 -10.0

Table 2—Continued

Model ¹	Parameters				\mathcal{R}_{tot} (Myr ⁻¹)			\mathcal{R}_{det} of LIGO (yr ⁻¹)			
	L_{min}^2 (mJy kpc ²)	p ³	R_0^4 (kpc)	Z_0^5 (kpc)	peak ⁷	68% ⁸	95% ⁸	initial peak ⁷ ($\times 10^{-3}$)	68% ⁸	advanced peak ⁷	68% ⁸
27	1.0	2.0	9.0 (G)	1.5 (E)	8.4	+10.0 -5.0	+25.1 -7.1	3.5	+4.2 -2.1	18.9	+22.6 -11.3

¹Model No.

²Minimum luminosity L_{min} in mJy kpc².

³Power index of the luminosity function p.

⁴Radial scale length R_o in kpc.

⁵Vertical scale height Z_o in kpc.

⁶Gaussian (G), and exponential (E) functions for spatial distributions.

⁷Peak value from $P(R_{\text{tot}})$.

⁸Confidence level.

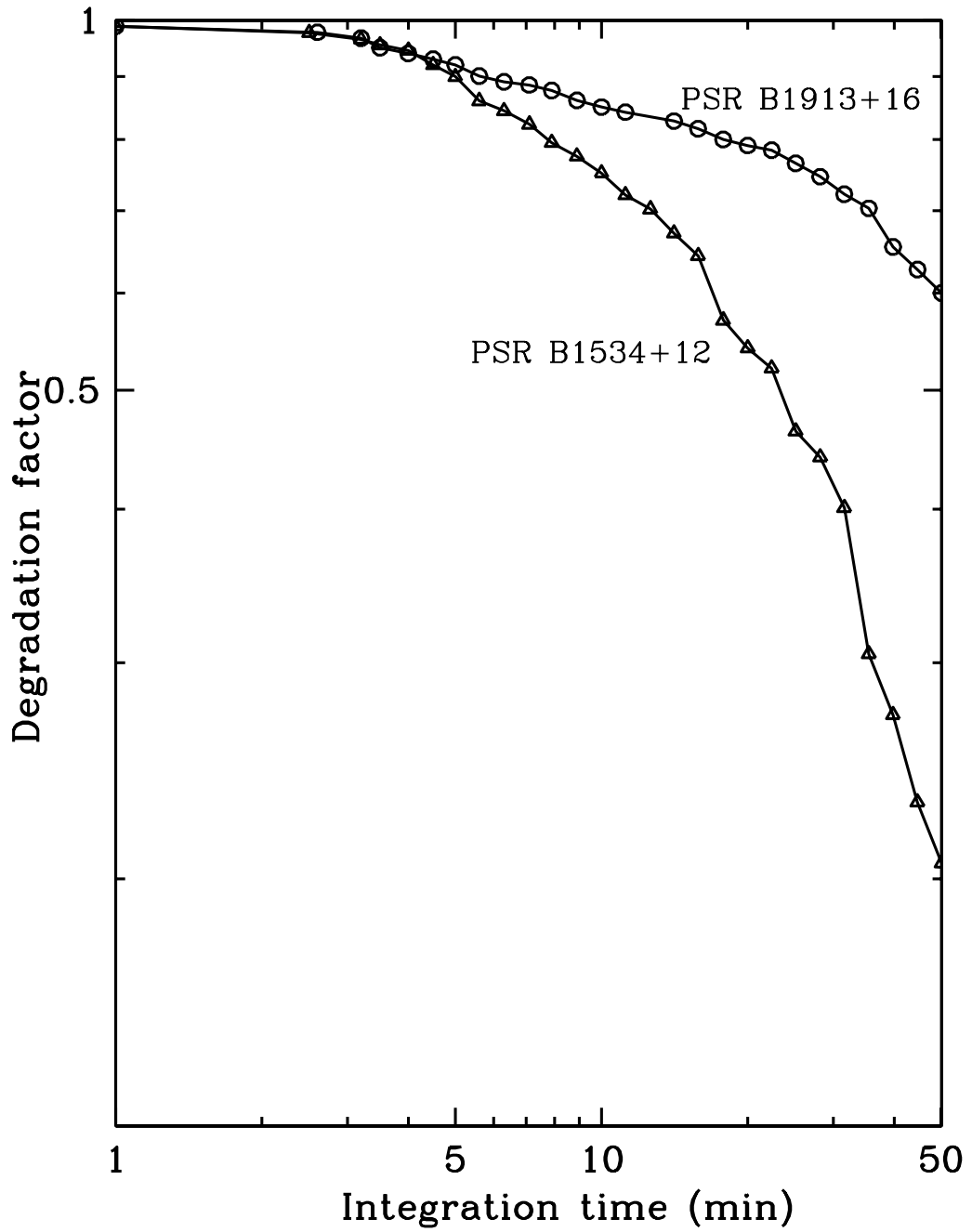


Fig. 1.— Average signal-to-noise degradation factor in pulsar search code versus survey integration time for PSR B1913+16 and PSR B1534+12.

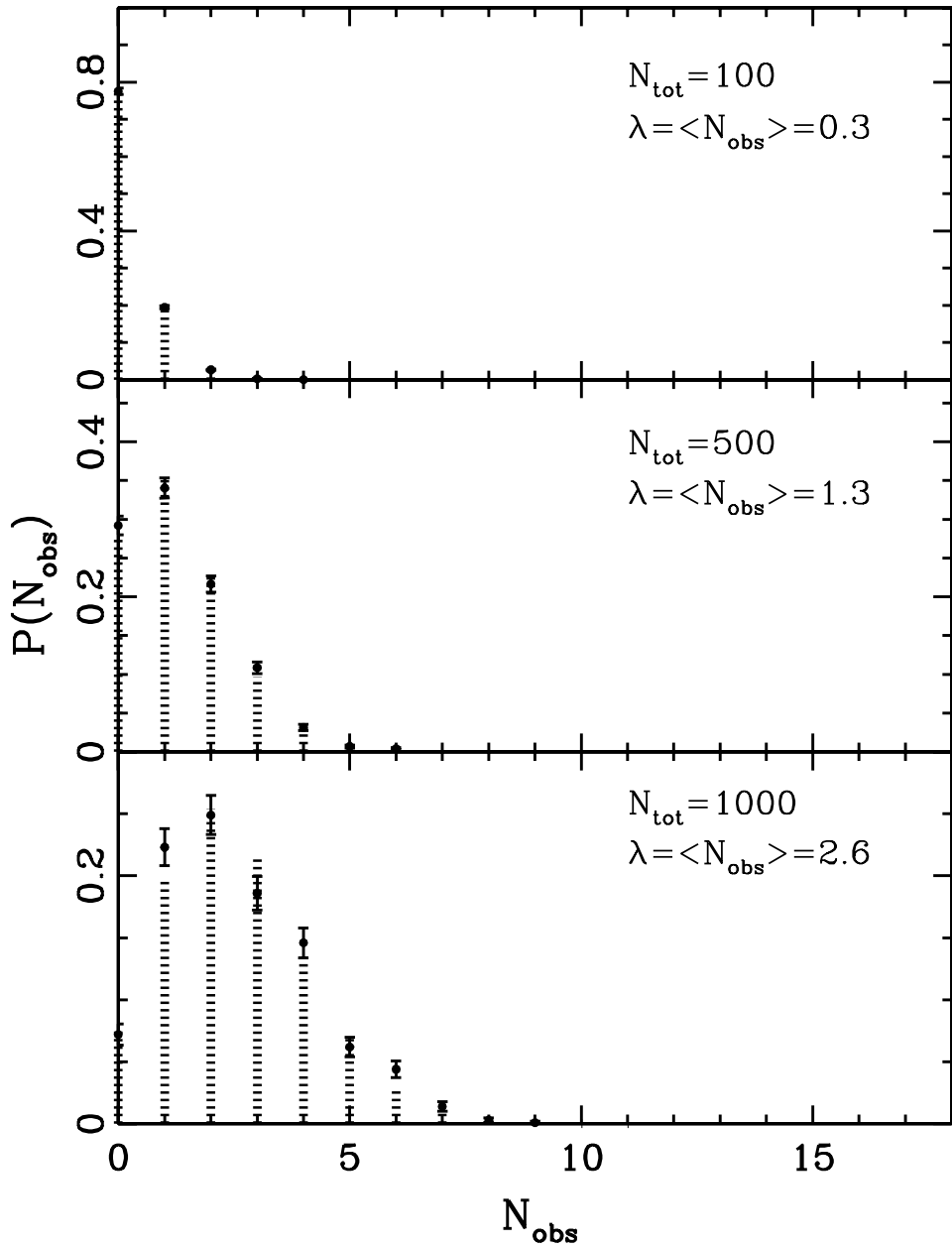


Fig. 2.— The Poisson-distribution fits of $P(N_{\text{obs}})$ for three values of the total number N_{tot} of PSR B1913+16-like pulsars in the Galaxy (results shown for model 1). Points and error bars represent the counts of model samples in our calculation. Dotted lines represent the theoretical Poisson distribution.

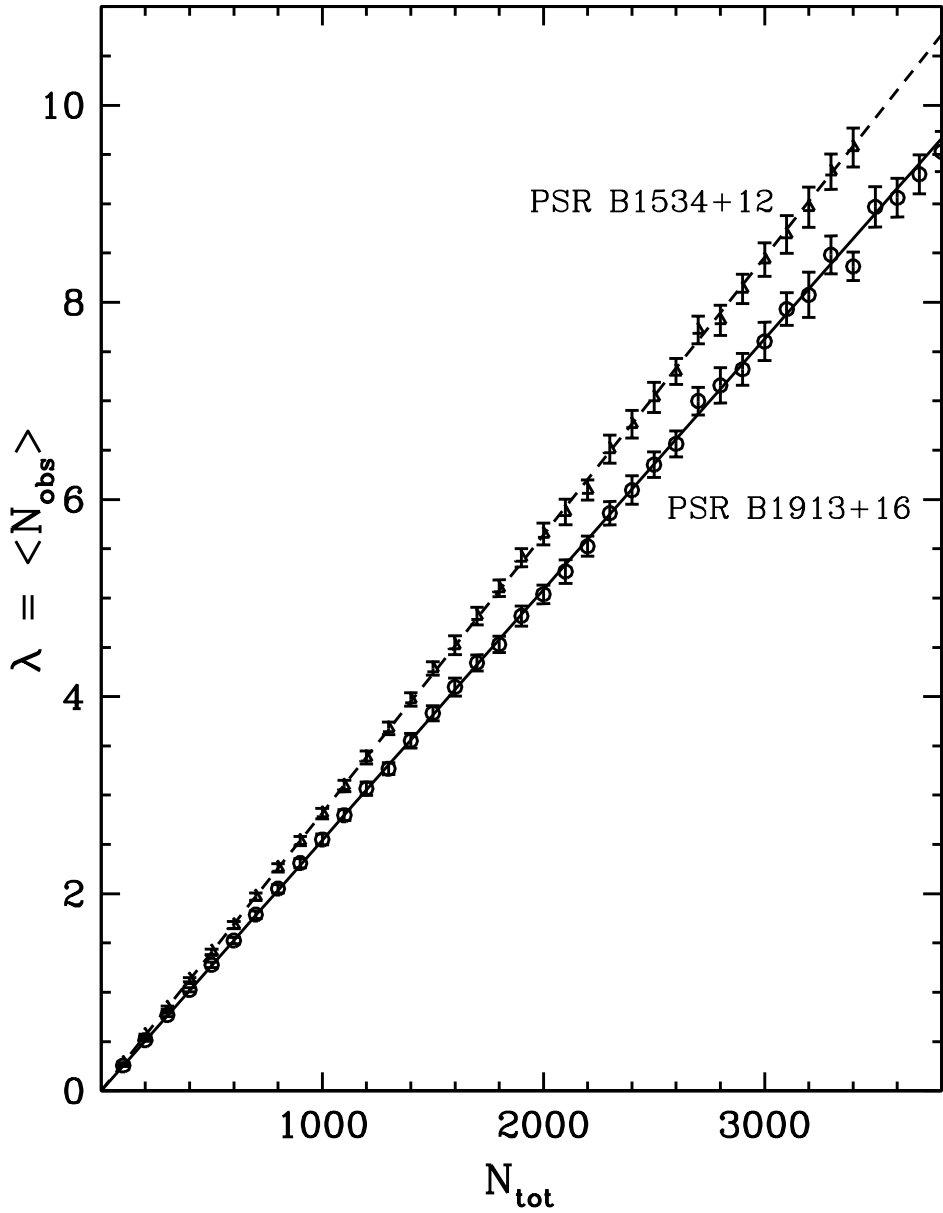


Fig. 3.— The linear correlation between $\lambda \equiv \langle N_{\text{obs}} \rangle$ and N_{tot} is shown for model 1. Solid and dashed lines are best-fit lines for PSR B1913+16-like and PSR B1534+12-like populations, respectively. Points and error bars represent the best-fit values of λ for different values of N_{tot} .

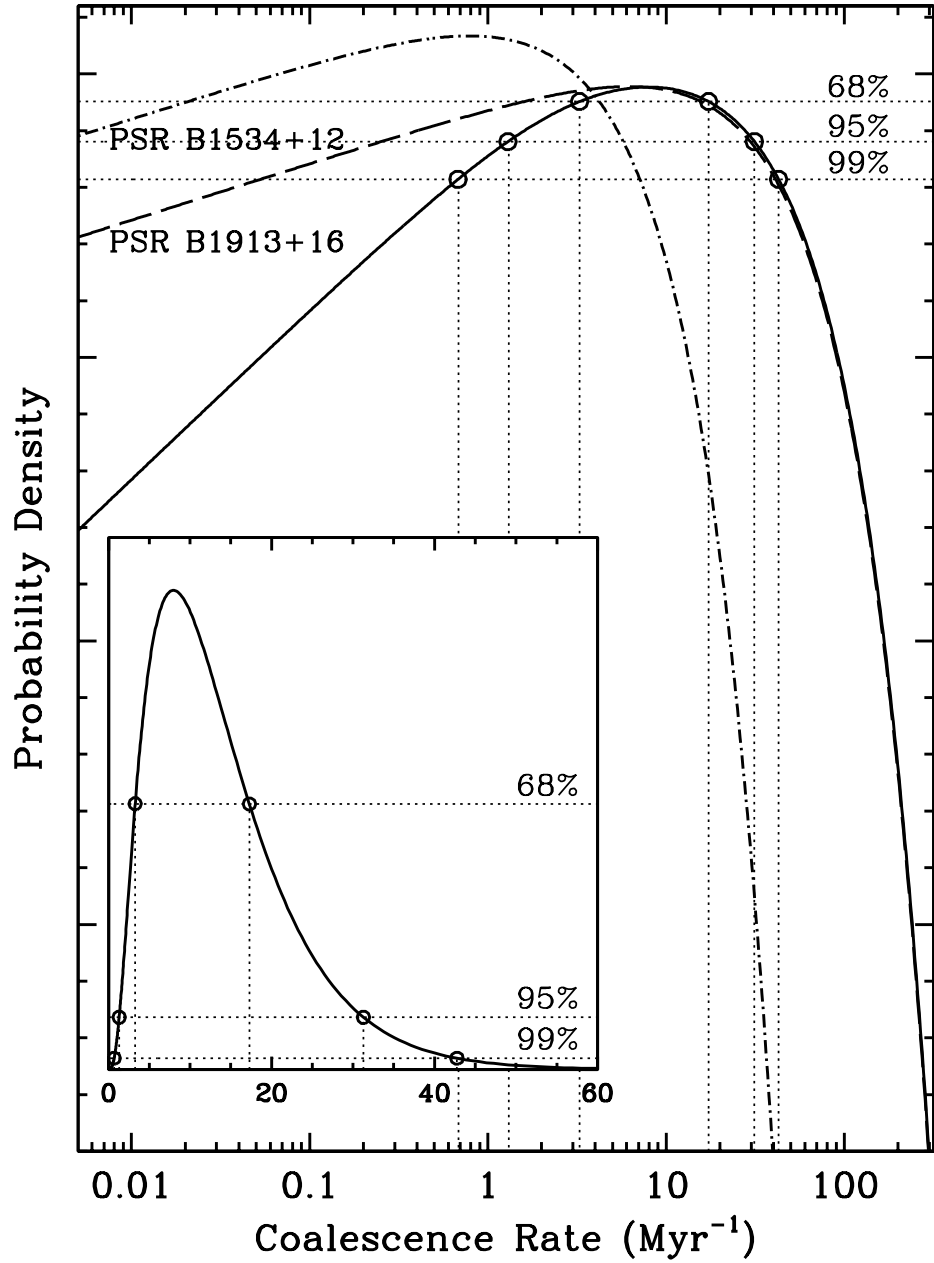


Fig. 4.— The probability distribution function of coalescence rates in both a logarithmic and a linear scale (small panel). The solid line represents $P(\mathcal{R}_{\text{tot}})$ and the long and short dashed lines represent $P(\mathcal{R})$ for PSR B1913+16-like and PSR B1534+12-like populations, respectively. We also indicate the confidence levels for $P(\mathcal{R}_{\text{tot}})$ by dotted lines.

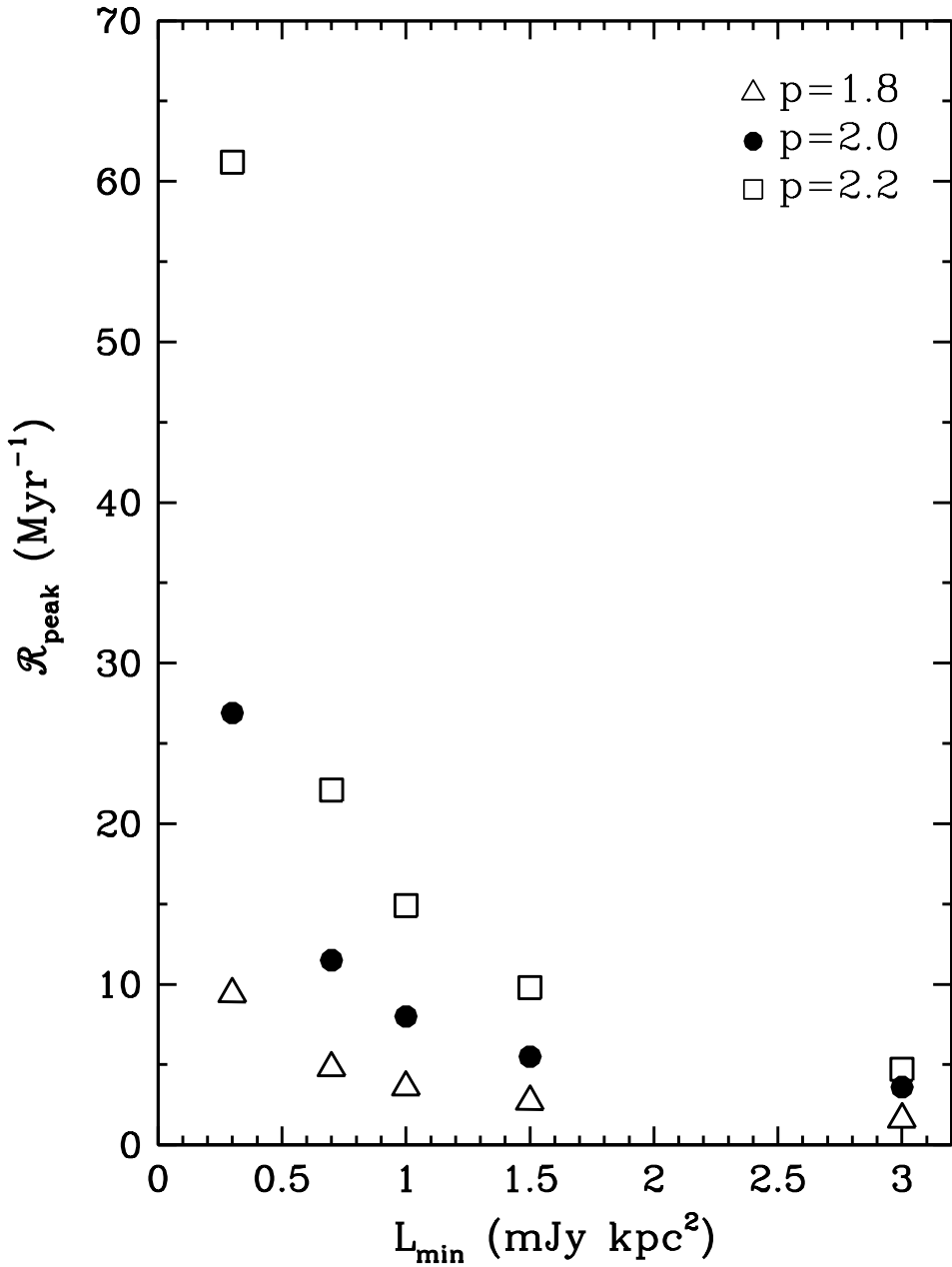


Fig. 5.— The correlation between $\mathcal{R}_{\text{peak}}$ and the cut-off luminosity L_{min} with different power indices p of the luminosity distribution function.

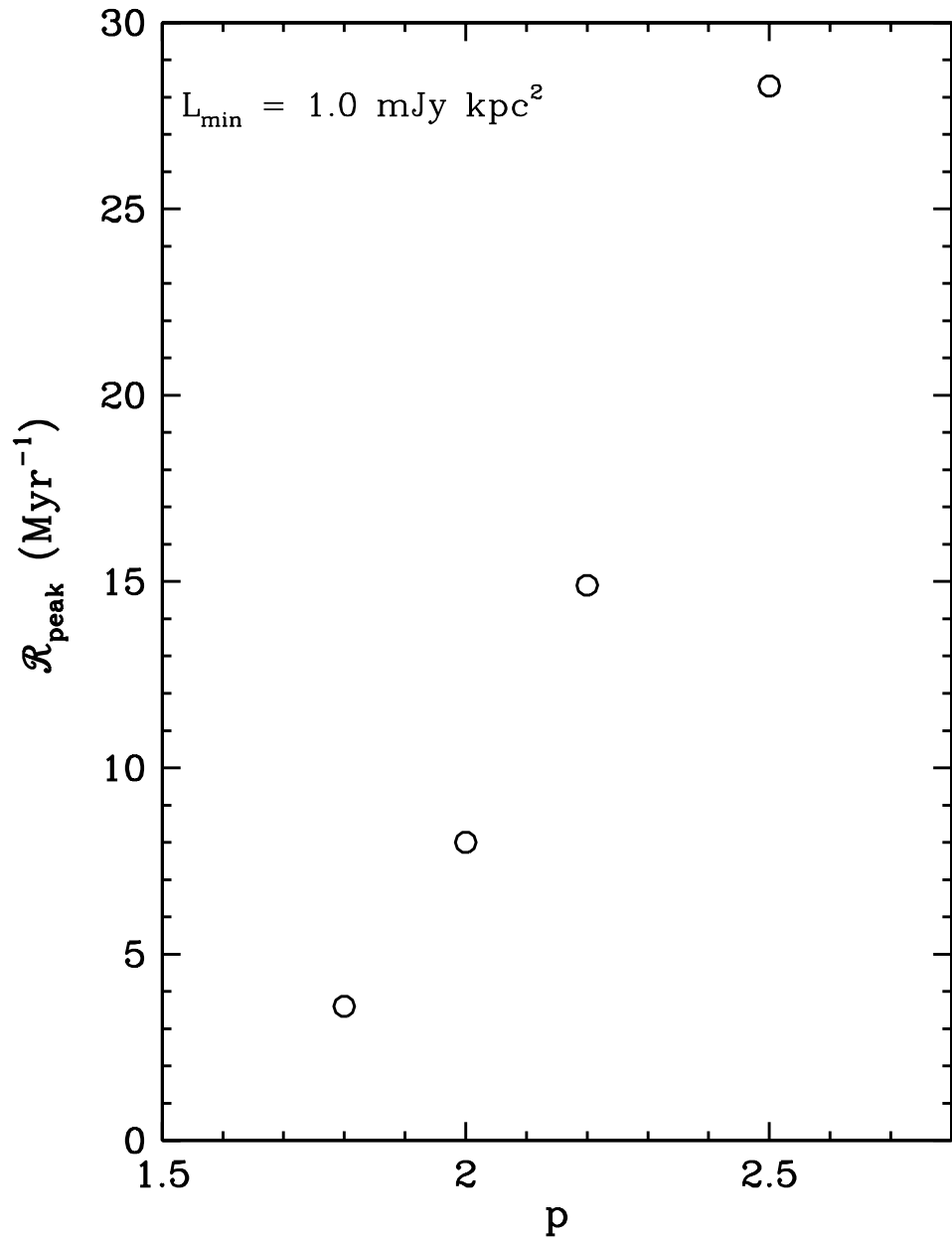


Fig. 6.— The correlation between $\mathcal{R}_{\text{peak}}$ and the power index of the luminosity distribution function p .

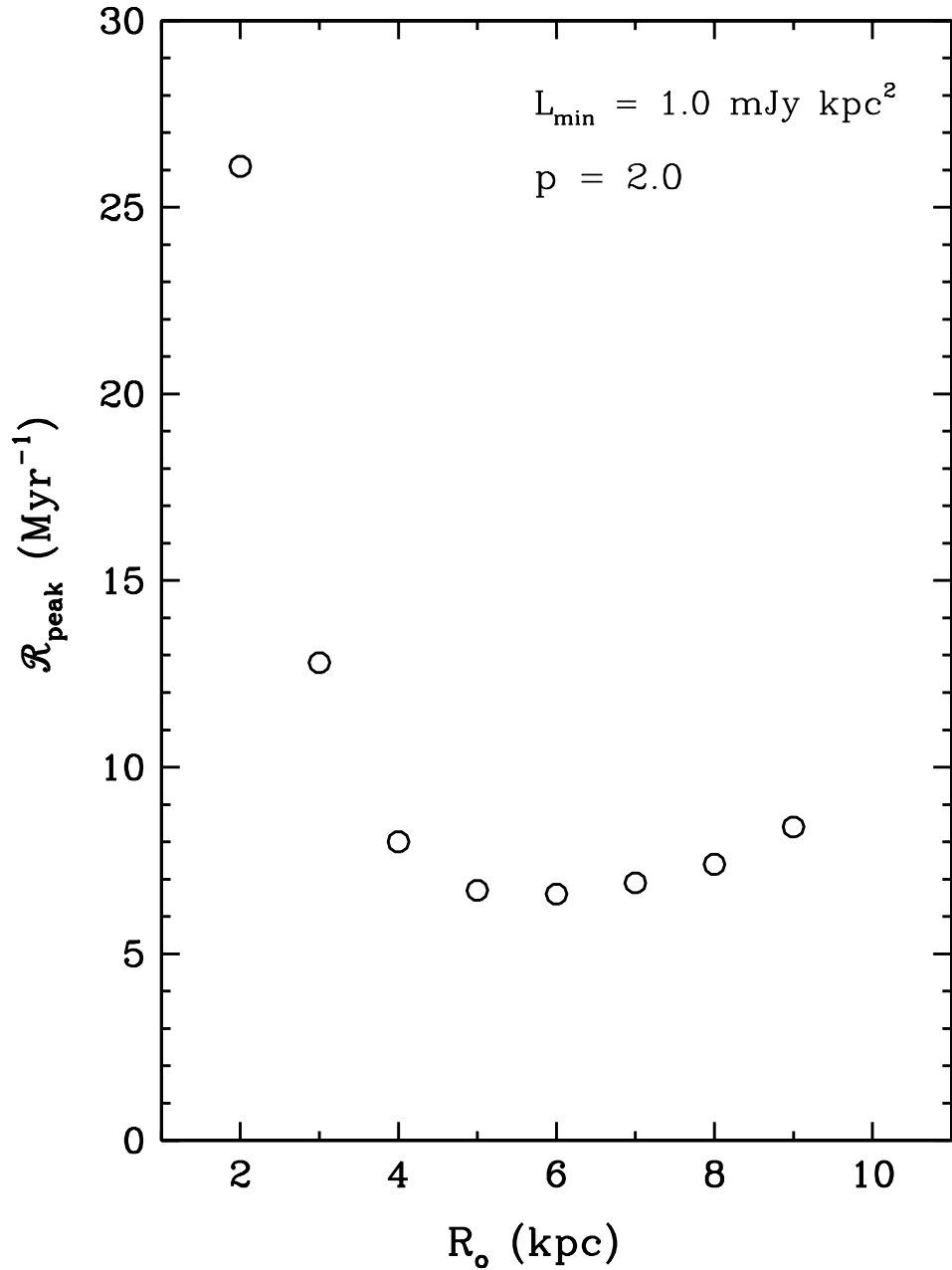


Fig. 7.— The correlation between $\mathcal{R}_{\text{peak}}$ and the radial scale length R_0 . $\mathcal{R}_{\text{peak}}$ is not sensitive to R_0 in the range between 4–9 kpc.